



Deposited via The University of Leeds.

White Rose Research Online URL for this paper:

<https://eprints.whiterose.ac.uk/id/eprint/127900/>

Version: Accepted Version

---

**Article:**

Besselink, R, Rodriguez-Blanco, JD, Stawski, TM et al. (2017) How Short-Lived Ikaite Affects Calcite Crystallization. *Crystal Growth & Design*, 17 (12). pp. 6224-6230. ISSN: 1528-7483

<https://doi.org/10.1021/acs.cgd.7b00743>

---

© 2017 American Chemical Society. This is an author produced version of a paper published in *Crystal Growth & Design*. Uploaded in accordance with the publisher's self-archiving policy.

**Reuse**

Items deposited in White Rose Research Online are protected by copyright, with all rights reserved unless indicated otherwise. They may be downloaded and/or printed for private study, or other acts as permitted by national copyright laws. The publisher or other rights holders may allow further reproduction and re-use of the full text version. This is indicated by the licence information on the White Rose Research Online record for the item.

**Takedown**

If you consider content in White Rose Research Online to be in breach of UK law, please notify us by emailing [eprints@whiterose.ac.uk](mailto:eprints@whiterose.ac.uk) including the URL of the record and the reason for the withdrawal request.

## How short-lived ikaite affects calcite crystallisation

R. Besselink, J. D. Rodriguez-Blanco, T. M. Stawski, L. G. Benning, and D. J. Tobler

*Cryst. Growth Des.*, **Just Accepted Manuscript** • DOI: 10.1021/acs.cgd.7b00743 • Publication Date (Web): 19 Sep 2017

Downloaded from <http://pubs.acs.org> on September 29, 2017

### Just Accepted

“Just Accepted” manuscripts have been peer-reviewed and accepted for publication. They are posted online prior to technical editing, formatting for publication and author proofing. The American Chemical Society provides “Just Accepted” as a free service to the research community to expedite the dissemination of scientific material as soon as possible after acceptance. “Just Accepted” manuscripts appear in full in PDF format accompanied by an HTML abstract. “Just Accepted” manuscripts have been fully peer reviewed, but should not be considered the official version of record. They are accessible to all readers and citable by the Digital Object Identifier (DOI®). “Just Accepted” is an optional service offered to authors. Therefore, the “Just Accepted” Web site may not include all articles that will be published in the journal. After a manuscript is technically edited and formatted, it will be removed from the “Just Accepted” Web site and published as an ASAP article. Note that technical editing may introduce minor changes to the manuscript text and/or graphics which could affect content, and all legal disclaimers and ethical guidelines that apply to the journal pertain. ACS cannot be held responsible for errors or consequences arising from the use of information contained in these “Just Accepted” manuscripts.



# How short-lived ikaite affects calcite crystallisation

R. Besselink<sup>a</sup>, J.D. Rodriguez-Blanco<sup>b, c</sup>, T. M. Stawski<sup>a</sup>, L.G. Benning<sup>a, d, e</sup> and D. J. Tobler<sup>b</sup>

<sup>a</sup>German Research Center for Geosciences, GFZ, Telegrafenberg, 14473, Potsdam, Germany

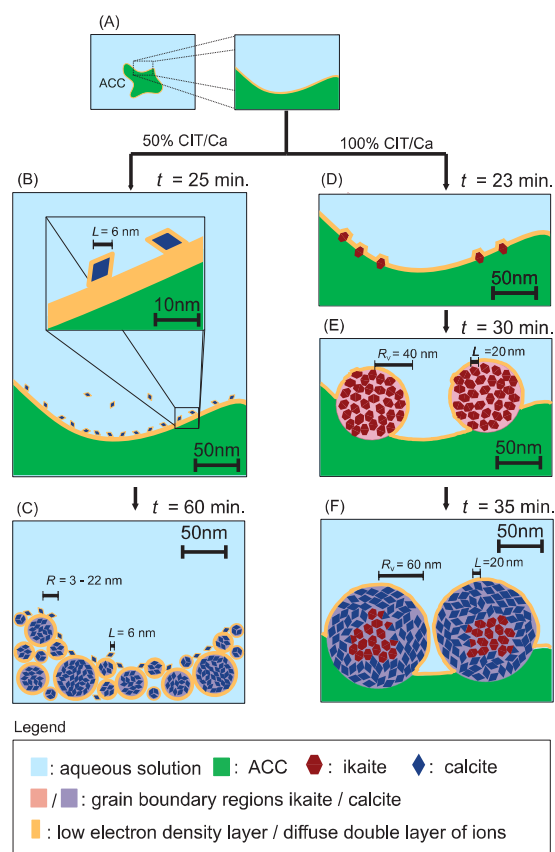
<sup>b</sup>Nano-Science Center, Department of Chemistry, University of Copenhagen, Copenhagen, Denmark

(\*Corresponding Author: dominique.tobler@nano.ku.dk)

<sup>c</sup>School of Natural Sciences, Department of Geology, Trinity College Dublin, Dublin, Ireland.

<sup>d</sup>Department of Earth Sciences, Free University of Berlin, 12249 Berlin, Germany

<sup>e</sup>School of Earth and Environment, University of Leeds, Leeds, United Kingdom



The pathways of  $\text{CaCO}_3$  crystallisation are manifold, often involving one or several metastable amorphous or nanocrystalline intermediate phases. The presence of such intermediates is often overlooked, because they are short-lived and/or occur at small molar fractions. However, their occurrence does not just impact the mechanisms and pathways of formation of the final stable  $\text{CaCO}_3$  phase, but also affects their crystal size, shape and structure. Here we document the presence of a short-lived intermediate through *in situ* and time-resolved small and wide angle X-ray scattering (SAXS/WAXS) combined with high resolution electron microscope observations. When ikaite forms concomitant with the dissolution of amorphous calcium carbonate (ACC) but prior to calcite formation, fairly large glendonite-type calcite crystals grow despite the presence of citrate ligands that usually reduce growth rate. These were ideal seeding crystals for further crystallization from supersaturated ions in solution. In contrast, in the absence of ikaite the crystallisation of calcite proceeds through transformation from ACC, resulting in fine-grained spherulitic calcite with sizes  $\approx 8$  times smaller than when ikaite was present. Noteworthy is, that the formation of the intermediate ikaite, although it consumes less than 3 mol % of the total precipitated  $\text{CaCO}_3$ , still clearly affected the calcite formation mechanism.

# How short-lived ikaite affects calcite crystallisation

*R. Besselink<sup>a</sup>, J.D. Rodriguez-Blanco<sup>b, c</sup>, T. M. Stawski<sup>a</sup>, L.G. Benning<sup>a, d, e</sup> and D. J. Tobler<sup>b</sup>*

<sup>a</sup>German Research Center for Geosciences, GFZ, Telegrafenberg, 14473, Potsdam, Germany

<sup>b</sup>Nano-Science Center, Department of Chemistry, University of Copenhagen, Copenhagen, Denmark

(\*Corresponding Author: dominique.tobler@nano.ku.dk)

<sup>c</sup>School of Natural Sciences, Department of Geology, Trinity College Dublin, Dublin, Ireland.

<sup>d</sup>Department of Earth Sciences, Free University of Berlin, 12249 Berlin, Germany

<sup>e</sup>School of Earth and Environment, University of Leeds, Leeds, United Kingdom

## Abstract

The pathways of  $\text{CaCO}_3$  crystallisation are manifold, often involving one or several metastable amorphous or nanocrystalline intermediate phases. The presence of such intermediates is often overlooked, because they are short-lived and/or occur at small molar fractions. However, their occurrence does not just impact the mechanisms and pathways of formation of the final stable  $\text{CaCO}_3$  phase, but also affects their crystal size, shape and structure. Here we document the presence of a short-lived intermediate through *in situ* and time-resolved small and wide angle X-ray scattering (SAXS/WAXS) combined with high resolution electron microscope observations. When ikaite forms concomitant with the dissolution of amorphous calcium carbonate (ACC) but prior to calcite formation, fairly large glendonite-type calcite crystals grow despite the presence of citrate ligands that usually reduce growth rate. These were ideal seeding crystals for further crystallization from supersaturated ions in solution. In contrast, in the absence of ikaite the crystallisation of calcite proceeds through transformation from ACC, resulting in fine-grained spherulitic calcite with sizes  $\approx 8$  times smaller than when ikaite was present. Noteworthy is, that the formation of the intermediate ikaite, although it consumes less than 3 mol % of the total precipitated  $\text{CaCO}_3$ , still clearly affected the calcite formation mechanism.

## Introduction

$\text{CaCO}_3$  minerals are widespread in nature where they play a pivotal role in biomineralisation processes and thus in the carbon cycle.<sup>1</sup> They are also important to industry where they are used for the production of paint, ceramics, paper, drugs, food supplements, abrasives etc.<sup>2</sup> In many natural systems  $\text{CaCO}_3$  crystallizes as the thermodynamically most stable polymorph calcite. However,  $\text{CaCO}_3$  crystallization pathways are diverse and complex because they are sensitive to many parameters, including temperature, pressure pH and the presence of impurities.<sup>3-5</sup> From a

1  
2  
3 kinetic point of view, it is very difficult to form highly symmetrical and completely dehydrated  
4 calcite through a simple reaction pathway. In contrast, metastable  $\text{CaCO}_3$  phases are often more  
5 easily formed, either reduced interfacial energy of metastable phases<sup>6</sup> or smaller degree of  
6 dehydration required for formation.<sup>7</sup>  
7  
8  
9  
10  
11

12 Understanding of  $\text{CaCO}_3$  crystallisation pathways, particularly when they involve one or more  
13 metastable precursor(s), is important because these pathways determine the size, shape and  
14 properties of the final stable calcite (or aragonite) crystals, found in soils, sediments, biominerals  
15 or synthesised in industrial processes. For example, when calcite forms following the breakdown  
16 of ACC, it commonly shows spherulitic morphologies.<sup>10-14</sup> This is explained by (1) a large  
17 solubility difference between the ACC and the crystalline polymorphs, and (2) the incorporation  
18 or adsorption of impurities blocking conventional calcite growth sites, leading to a nucleation  
19 controlled growth mechanism and formation of intertwined nanocrystals.<sup>4,5,8,9</sup> In contrast, when  
20 calcite forms through pseudomorphic transformation of ikaite, it exhibits the characteristic  
21 bipiramidal or hedgehog shaped morphology of ikaite, commonly described as glendonite.<sup>15-18</sup>  
22 While the ikaite shape is preserved in this transformation to calcite, the molar volume is  
23 substantially reduced, by 76% (ikaite: ISCD 31305<sup>19</sup> and calcite: AMSCD 0000098<sup>20</sup>). As a  
24 result glendonites are highly porous, and they also often retain some of the ikaite structural water  
25 within the newly formed calcite crystal.<sup>18,20</sup>  
26  
27  
28  
29  
30  
31  
32  
33  
34  
35  
36  
37  
38  
39  
40  
41  
42  
43  
44  
45

46 These examples give a small glimpse into the large diversity in  $\text{CaCO}_3$  crystallization  
47 pathways and show how minute changes can affect the properties of the stable end material,  
48 including porosity, grain size, mechanical strength, morphology, etc. Understanding, these  
49 mechanisms at the nanoscale is key towards designing tailor-made  $\text{CaCO}_3$  polymorphs for  
50 various industrial applications. Furthermore, being able to understand how the crystallization  
51  
52  
53  
54  
55  
56  
57  
58  
59  
60

1  
2  
3 history is preserved in the final observed  $\text{CaCO}_3$  polymorph, helps to reconstruct its formation  
4  
5 conditions. For example, porous glendonite polymorphs are paleoclimatic indicators of low-  
6  
7 temperature condition, under which ikaite was formed.<sup>21</sup>  
8  
9

10 Here, we investigated the role that short-lived ikaite has during the formation of calcite via  
11  
12 ACC by means of synchrotron based small and wide angle X-ray scattering at temperatures  
13  
14 between 2 and 12 °C. In our previous study, we documented that in the presence of magnesium<sup>22</sup>  
15  
16 or citrate,<sup>23</sup> ACC directly crystallises to calcite, with no vaterite intermediate. We used here a  
17  
18 similar set-up to the above mentioned citrate study but ran the experiments at a lower  
19  
20 temperatures to facilitate ikaite formation. We discovered that only a high citrate (CIT)  
21  
22 concentration (CIT/Ca = 100%) facilitated the formation of ikaite besides ACC, yet that this was  
23  
24 short-lived. In contrary, at lower citrate concentration (CIT/Ca = 50%) ACC transformed directly  
25  
26 into calcite without the ikaite intermediate. Although ikaite formation was short-lived and  
27  
28 included < 3 mol% of the total precipitated  $\text{CaCO}_3$ , it strongly changed the calcite crystallization  
29  
30 mechanism and kinetics and led to the growth of far larger calcite crystals.  
31  
32  
33  
34  
35  
36  
37  
38  
39  
40  
41

## 42 **Methods**

43  
44 The formation and crystallization of  $\text{CaCO}_3$  phases was studied in the presence of citrate (CIT;  
45  
46  $\text{C}_6\text{H}_5\text{O}_7^{3-}$ ) by mixing equal volumes of a 0.05 M  $\text{CaCl}_2$  solution and a 0.05 M  $\text{Na}_2\text{CO}_3$  solution  
47  
48 with either 0.025 or 0.050 M monohydrate citric acid (corresponding to 50 or 100% CIT/Ca).  
49  
50 Stock solutions were prepared using reagent grade chemicals and ultrapure deionized water  
51  
52 (MilliQ, resistivity > 18 M $\Omega$  cm). CIT-containing carbonate solutions were pH adjusted to 11.2  
53  
54 (2 M NaOH) to match the pH of the pure  $\text{Na}_2\text{CO}_3$  solution. The formation and crystallization of  
55  
56  
57  
58  
59  
60

1  
2  
3 CaCO<sub>3</sub> phases was followed *in situ* and in a time-resolved mode by using small- and wide-angle  
4 X-ray scattering (SAXS/WAXS) at beamline I22 at the Diamond Light Source Ltd. (UK). For  
5 each experiment, equal volumes of the calcium and CIT-containing carbonate solution, both pre-  
6 cooled to 5 °C, were injected into a 3-neck reactor flask (250 mL) using a remotely controlled  
7 peristaltic pump (Gilson Mini Puls 3) at 200 mL/min. The resulting mixed liquid/suspension was  
8 continuously stirred at 300 rpm and circulated at a flow rate of 50 mL/min through a flow-  
9 through cell containing a borosilicate glass capillary (d = 1.5 mm) that was aligned perpendicular  
10 to the X-ray beam. To avoid rapid warming up of the solution to the temperature of the beamline  
11 hutch (21 °C), the reactor was placed in a pre-cooled oil bath with an initial temperature of 1 °C.  
12 After 1 hour the solutions reached a temperature of 14 °C and a typical time trend for the change  
13 in solution temperature during an experiment is shown in Figure 1A.  
14  
15  
16  
17  
18  
19  
20  
21  
22  
23  
24  
25  
26  
27  
28

29 SAXS/WAXS data were acquired by using a monochromatic X-ray beam at 16 keV. Two-  
30 dimensional SAXS intensities were collected with a Dectris Pilatus 2M (2D large area pixel-  
31 array detector<sup>24</sup>). Transmission was measured by means of a photodiode installed in the beam-  
32 stop of the SAXS detector. A sample-to-detector distance of 9.22 m allowed for a usable q-range  
33 of  $0.055 < q < 2.187 \text{ nm}^{-1}$ . The scattering-range at small-angles was calibrated against silver  
34 behenate<sup>25</sup> and dry collagen standards.<sup>26</sup> In all the cases the recorded 2D scattering patterns were  
35 reduced to 1D scattering curves, normalised and corrected for transmission, and background-  
36 corrected. For background subtraction we used a scattering from a cell filled with water. The  
37 intensity scale was calibrated to absolute units by using a glassy carbon reference.<sup>27</sup> Data  
38 acquisition was performed in experiments that lasted for up to 2 hours and spectra were recorded  
39 at a time resolution of 30 seconds per frame.  
40  
41  
42  
43  
44  
45  
46  
47  
48  
49  
50  
51  
52  
53  
54  
55  
56  
57  
58  
59  
60

1  
2  
3 Simultaneously, two-dimensional WAXS intensities were collected with a DecriS Pilatus 300k  
4 detector (2D large-area pixel array detector,<sup>24</sup> which was calibrated with synthetic and highly  
5 crystalline silicon (NIST SRM 640C). This silicon standard was used to determine the  
6 instrumental broadening ( $\Delta q_{\text{instrument}} = 0.17 \text{ nm}^{-1}$ ) and the corrected peak width ( $\Delta q_{\text{corrected}}^2 =$   
7  $\Delta q_{\text{measured}}^2 - \Delta q_{\text{instrument}}^2$ ) was used to determine crystallite size by the Scherrer equation.<sup>28</sup> The  
8 WAXS detector covered the  $q$ -range of  $23.9 < q < 38.7 \text{ nm}^{-1}$ . All recorded patterns were  
9 normalised and background-corrected using water. For all samples a broad correlation peak with  
10 a maximum at  $q \approx 29 \text{ nm}^{-1}$  remained present, which we related to typical Ca-O distances within  
11 ACC:  $d \approx 0.24 \text{ nm}$ .<sup>23</sup> The shape of this amorphous background was determined over the initial 10  
12 frames, averaged, smoothed and subtracted from the subsequent frames in the ratios individually  
13 optimized for all frames.  
14  
15  
16  
17  
18  
19  
20  
21  
22  
23  
24  
25  
26  
27  
28

29 A Principal Component Analysis (PCA) procedure from PTC Mathcad v15.0 was used to  
30 determine these ratios, as well as to identify the contributions from crystalline  $\text{CaCO}_3$  phases  
31 present in the diffraction signal. This procedure allowed us to describe a large dataset based on a  
32 limited set of principal components. Every principal component was represented by a vector of  
33 scores and loadings. The score vectors represent characteristic diffraction patterns of a principal  
34 component, which in our experiments were assigned to pure  $\text{CaCO}_3$  phases (e.g., calcite, ikaite).  
35 The loading vectors represent the contribution of a given phase at various reaction times. These  
36 contribution profiles were normalised against the overall peak area and the number of electrons  
37 per formula unit of ikaite and calcite, so that the ratio between both profiles was proportional to  
38 their molar ratio.  
39  
40  
41  
42  
43  
44  
45  
46  
47  
48  
49  
50  
51  
52  
53  
54  
55  
56  
57  
58  
59  
60

The final precipitates from the *in situ* and real-time experiments were separated from the solutions by using vacuum filtration, then rinsed with isopropanol to remove remaining water and quickly dried by blowing air over the solids. Powder X-ray diffraction (XRD, Bruker D8, Co  $K\alpha_{1,2}$  radiation,  $0.02^\circ$  from  $10$  to  $70^\circ$   $2\theta$ ,  $1^\circ \text{ min}^{-1}$ ) was used to verify the nature of the  $\text{CaCO}_3$  phases present at the end of the experiment, while scanning electron microscopy (SEM, FEI Quanta 3D, 5 kV) and transmission electron microscopy (TEM, Phillips CM 20, 20 kV) were utilized to characterize their crystal size and morphology.

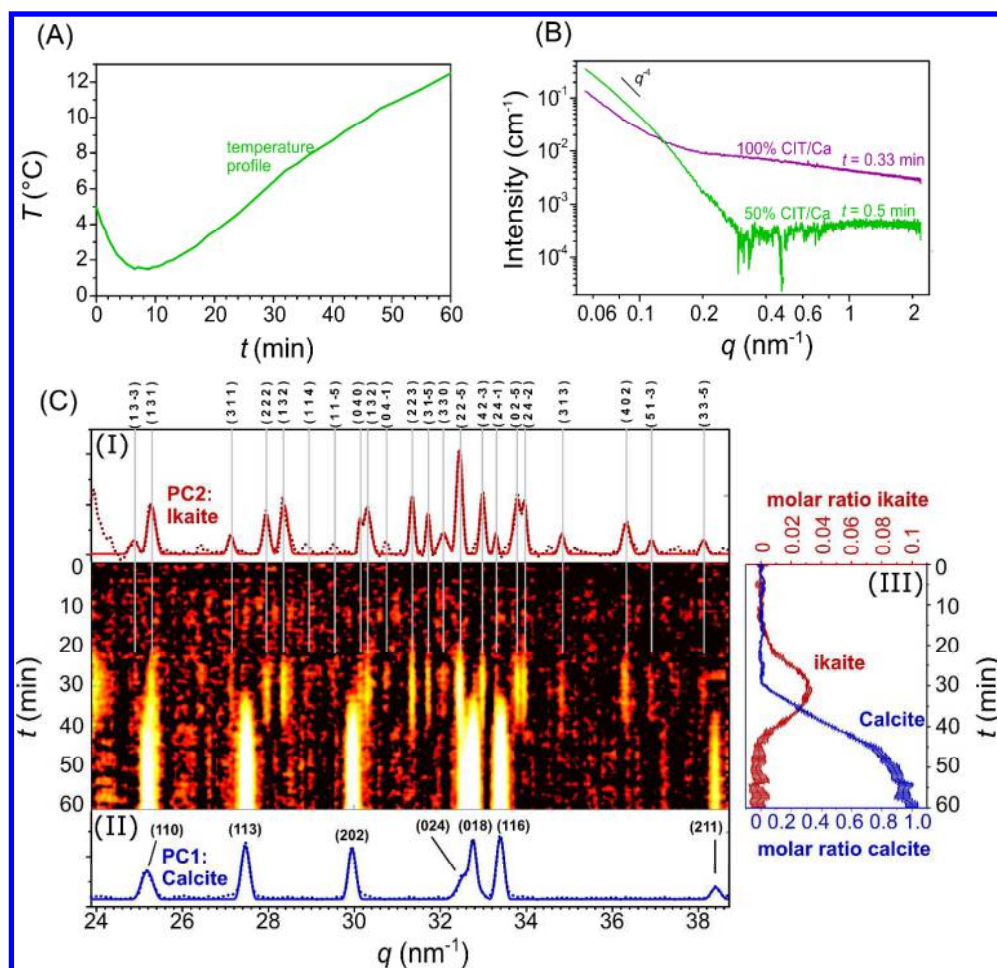


**Figure 1.** (A) Solution temperature as a function of experimental reaction time. (B) SAXS patterns of  $\text{CaCO}_3$  suspensions 0.5 and 0.33 min after mixing for 50% and 100% CIT/Ca

1  
2  
3 respectively, (C) 2D WAXS intensity map for 100% CIT/Ca with the scale increasing from black  
4 to red, orange, yellow and white, with  $q$ -spacing ( $\text{nm}^{-1}$ ) on the horizontal axis and reaction time  
5 (min) on the vertical axis. This set of WAXS scattering intensities was deconvoluted by means of  
6 principal component analysis into two characteristic patterns, namely: (I) the WAXS pattern of  
7 principal component 2 was assigned to ikaite (see Miller indices) and (II) the WAXS pattern of  
8 principal component 1 was assigned to calcite (see Miller indices), where (III) represents the  
9 time resolved molar ratios of ikaite and calcite with respect to calcite at  $t = 60$  min. Please note  
10 that ikaite and calcite molar ratios are scaled on separate Y-axes.  
11  
12  
13  
14  
15  
16  
17  
18  
19  
20  
21  
22

## 23 Results and Discussion

24  
25  
26 For the tested CIT/Ca ratios, ACC formed within the first 30 seconds after solution mixing as  
27 indicated by the sharp increase to  $I \propto q^4$  in the SAXS intensity in the low- $q$  regime (for  $q < 1$   
28  $\text{nm}^{-1}$  Figure 1B) and the absence of any crystalline phases in the WAXS pattern (Figure 1C).  
29 Since this curve does not level off for lower  $q$ -values within the measured range, the particles  
30 within these suspensions must have reached particle radii larger than 50 nm ( $\approx \pi / q_{\text{min}}$ ). XRD  
31 analyses performed on these initial precipitates (prepared offline, under identical conditions)  
32 confirmed that the ACC material was characterized only by the presence of broad correlation  
33 peaks in the patterns.  
34  
35  
36  
37  
38  
39  
40  
41  
42  
43  
44

45 The so formed ACC remained stable for approximately 20 minutes prior to crystalline  $\text{CaCO}_3$   
46 formation. From our previous work<sup>23</sup> we had expected that in the presence of CIT, ACC would  
47 crystallize directly to calcite, which indeed we observed for the 50% CIT/Ca experiment (Figure  
48 2A). However, in the 100% CIT/Ca experiment, the time-resolved WAXS pattern (Figure 1C)  
49 showed the presence of two separate crystalline phases distinguished by the PCA analyses that  
50 could be assigned to ikaite (Figure 1C-I) and calcite (Figure 1C-II), respectively. In this  
51  
52  
53  
54  
55  
56  
57  
58  
59  
60

1  
2  
3 experiment, we observed the formation of ikaite at  $t = 20$  min (Figure 1C, 2A), when ACC  
4 presumably started to dissolve.<sup>29</sup> Once formed, Ikaite continued to increase in volume fraction up  
5  
6 to  $t = 30$  min, after which calcite started to appear (Figure 1C, 2A). Thereafter, calcite steadily  
7  
8 increased in its volume fraction concomitant with the decrease in ikaite volume fraction. This  
9  
10 decrease lasted until  $t = 42$  min, after which no more ikaite was detected. Nevertheless, calcite  
11  
12 further increased in its volume fraction until  $t = 60$  min. The matrix contribution profiles of  
13  
14 calcite and ikaite (as obtained from PCA, Figure 1C-III, 2A) were normalised against the overall  
15  
16 peak area and the number of electrons per formula unit, so that the ratio between both profiles  
17  
18 was proportional to their molar ratio.  
19  
20  
21  
22  
23  
24  
25  
26  
27  
28  
29  
30  
31  
32  
33  
34  
35  
36  
37  
38  
39  
40  
41  
42  
43  
44  
45  
46  
47  
48  
49  
50  
51  
52  
53  
54  
55  
56  
57  
58  
59  
60

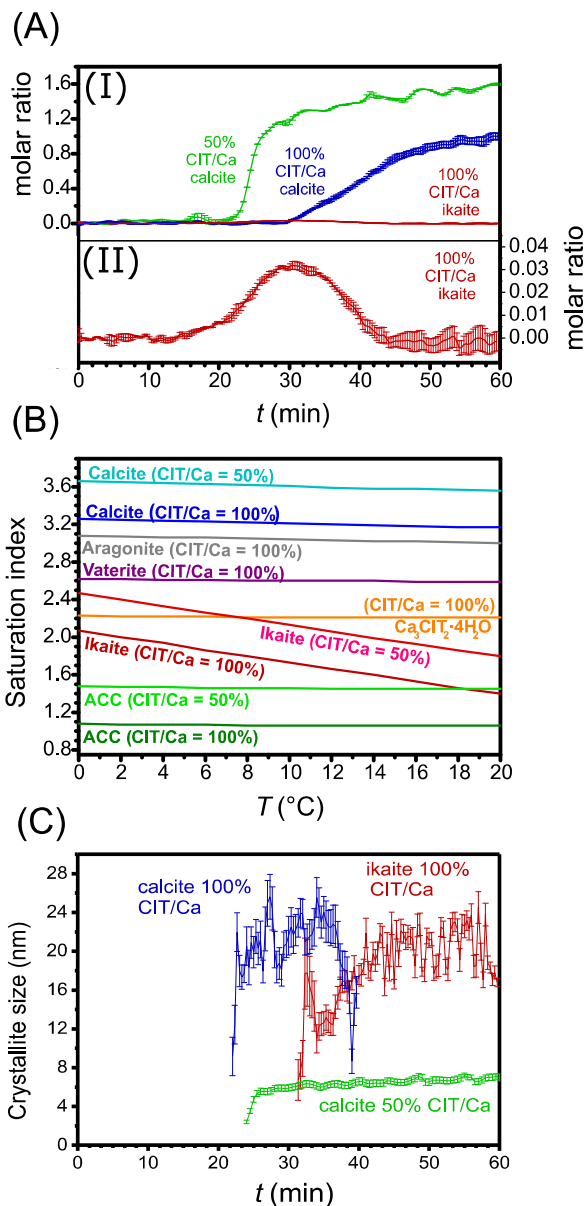


**Figure 2.** (A-I) Time resolved molar ratios of ikaite and calcite for both 50% and 100% CIT/Ca, with respect to 100% CIT/Ca at  $t = 60$  min. This was quantified by multiplying the contribution of a given principal component with the WAXS peak areas of the corresponding principal component, subsequently normalised against the number of moles electrons per molar unit of a given polymorph, and finally normalised against 100% CIT/Ca at  $t = 60$  min. (A-II) Amplified graph for the molar ratio of Ikaite for 100% CIT/Ca (B) Saturation indices for calcium carbonate

1  
2  
3 polymorphs and  $\text{Ca}_3\text{CIT}_2 \cdot 4\text{H}_2\text{O}$ . Saturation indices were calculated with PHREEQC<sup>30</sup> by using  
4  
5 temperature dependent solubility products for calcite, vaterite and aragonite from<sup>31</sup> and for ACC  
6  
7 from<sup>32</sup>. (C) Crystallite size of calcite for both 50 and 100% CIT/Ca (PC1) and ikaite for 100%  
8  
9 CIT/Ca (PC2) by using the Scherrer equation obtained from the time-resolved WAXS patterns.  
10  
11  
12  
13  
14  
15

16  
17 Consequently, the maximum molar fraction of ikaite present at  $t = 30$  min could be estimated  
18  
19 to be approximately 3% of the final amount of calcite (at  $t = 60$  min). Moreover, by comparing  
20  
21 the changes in molar ratios between calcite and ikaite (Figure 2A), we could estimate the  
22  
23 percentage of calcite that formed directly as a result of the breakdown of ikaite. If we consider  
24  
25 the 10 time frames spanning  $t = 35$  and 40 min, we observe that the maximum rate of ikaite  
26  
27 depletion is still 15 times lower than the rate of calcite formation. In terms of molar ratios only  
28  
29 6.4 % of the  $\text{CaCO}_3$  used for calcite formation were derived from ikaite, while the remaining  
30  
31 93.6 % formed either from ACC or from the remnant supersaturated ions in the reacting solution.  
32  
33  
34  
35

36  
37 A comparison between both experiments revealed a three times larger initial rate of calcite  
38  
39 formation for the 50% CIT/Ca ratio compared to the 100% CIT/Ca experiment (Figure 2A). In  
40  
41 part, this is explained by the difference in the saturation indices, which at  $T = 4^\circ\text{C}$  are 3.64 and  
42  
43 3.24 for calcite at CIT/Ca ratios of 50% and 100%, respectively (Figure 2B). Additionally, it has  
44  
45 been shown that citrate slows down both calcite nucleation and growth through adsorption, thus  
46  
47 at the higher citrate concentration, calcite crystallization was hindered to a larger extent, leading  
48  
49 to a slower calcite crystallisation rate. In addition, the calcite crystallite sizes were smaller at  
50  
51 50% CIT/Ca ( $L \approx 6$  nm) compared to 100% CIT/Ca ( $L \approx 18$  nm, Figure 2C). This size difference  
52  
53 may be explained by a reduced nucleation rate for an increased CIT/Ca ratio and/or a different  
54  
55 crystallisation mechanism at 100% CIT/Ca, given the presence of ikaite. Although the presence  
56  
57  
58  
59  
60

of citrate reduces calcite crystallisation rates, this does not seem to affect the calcite crystal size, as shown in recent work.<sup>33</sup> Calcite crystals became more elongated with increasing CIT/Ca, showing preferential growth in one direction due to citrate adsorption at  $\{10\bar{1}4\}$  steps, while the crystal volume remained constant.

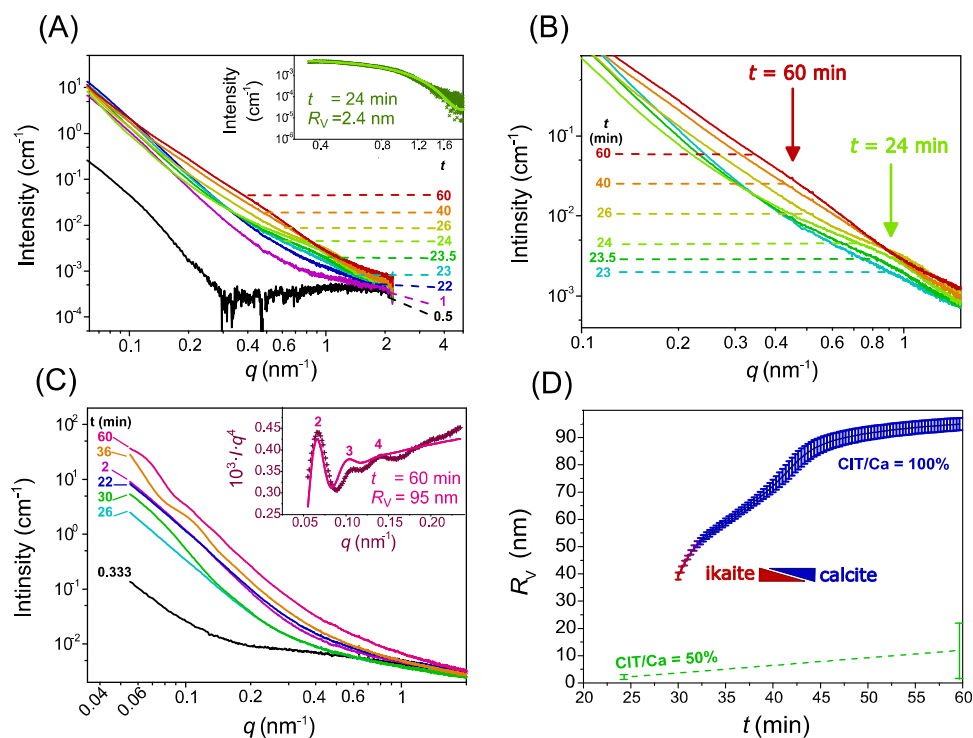


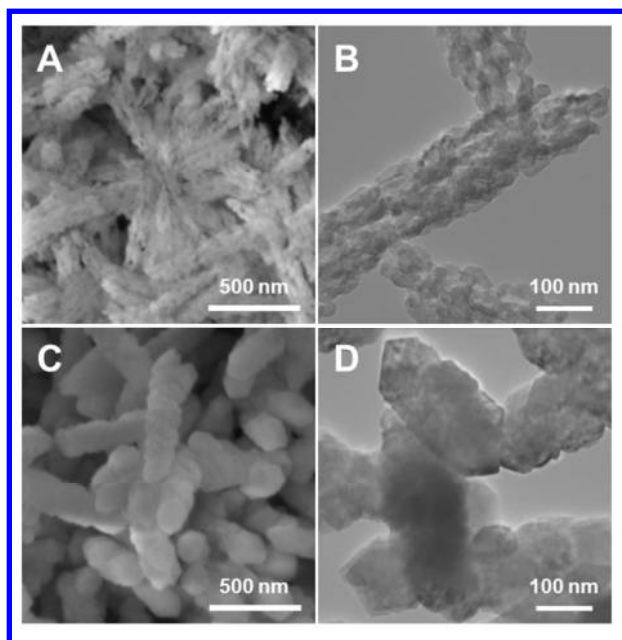
**Figure 3.** (A) This procedure revealed the presence of small solid particles with a radius  $R_V = 2.4$  nm, (B) Zoom in of SAXS pattern in a to emphasize the shift in the lobe to lower  $q$ -values for increasing reaction times, the green and red arrows point to the bending point of lobes for  $t = 23.5$  and 60 min respectively (C) “Selected SAXS patterns at various times after mixing for the 50% CIT/Ca experiment: the inset shows a SAXS pattern derived for the data at  $t = 24$  min, from which the scattering at  $t = 22$  min was subtracted, and this curve was fitted with a spherical form

1  
2  
3 function, which included polydispersity with the Schultz-Zimm distribution.<sup>34</sup> (D) Volume  
4 averaged particle size,  $R_v$ , obtained from time resolved SAXS patterns.  
5  
6  
7

8  
9  
10 As mentioned above, no ikaite peaks were detected in WAXS patterns of the 50% CIT/Ca  
11 experiment. The direct transition from ACC to calcite is likely a result of ACC dissolution and  
12 nucleation and growth of calcite from solution. This is also suggested by the SAXS pattern from  
13 this experiment (Figure 3A), which showed the appearance of a new lobe with a bending or knee  
14 point at  $q \approx 0.8 \text{ nm}^{-1}$  for  $t = 24 \text{ min}$ . This is indicative of an additional nucleation event, which in  
15 this experiment coincides with the nucleation of calcite. Fitting of this lobe revealed a volume  
16 averaged spherical particle radius of  $R_v = 2.4 \text{ nm}$  at  $t = 24 \text{ min}$  (inset in Figure. 3A). This size  
17 may be close to the critical nucleus size of calcite, which seems consistent with molecular  
18 dynamic calculations which suggested that at a diameter below 3.8 nm calcite becomes  
19 thermodynamically unfavourable with respect to ACC with an optimal hydration ratio.<sup>35</sup> As  
20 crystallization continues, these particles increased both in size and polydispersity as shown by  
21 the shift to lower  $q$ -values and the broadening of the lobe (see arrows Figure 3B).  
22  
23  
24  
25  
26  
27  
28  
29  
30  
31  
32  
33  
34  
35  
36  
37

38 One second before the onset of calcite crystallisation at  $t = 30 \text{ min}$  for the 100% CIT/Ca  
39 experiment, a lobe with a bending point at  $q \approx 0.075 \text{ nm}^{-1}$  appeared in SAXS-pattern (Figure  
40 3C), which corresponded to presumably ikaite particles with a size of  $R_v \approx 40 \text{ nm}$ . We did not  
41 observe such particles in an earlier stage despite the fact that ikaite was already observed after 20  
42 min, possibly due to an insufficient volume fraction of ikaite with respect to the ACC particle,  
43 that may dominate the SAXS patterns at earlier time frames. Moreover, these particles may be  
44 partially composed of ACC, but calcite was still absent at this stage.  
45  
46  
47  
48  
49  
50  
51  
52  
53  
54  
55  
56  
57  
58  
59  
60

1  
2  
3 For increasing reaction times, as ikaite transforms to calcite, this lobe shifted to lower  $q$ -values  
4 corresponding to increasing particle sizes and lobes appeared in the patterns which positions  
5 corresponded to higher order oscillations of the same presumably spheroidal particles (see curve  
6 of  $t = 36$  and  $60$  min Figure 3C and inlet). Meanwhile no new lobes appeared at lower  $q$ -range ( $q$   
7  $> 0.2 \text{ nm}^{-1}$ ) in this experiment at the onset of calcite formation. Thus as calcite formed in the  
8 100% CIT/Ca experiment, its particle size remained fairly large ( $R_V > 40 \text{ nm}$ ) compared to the  
9 50% CIT/Ca experiment ( $3 \leq R_V \leq 22 \text{ nm}$ ) as illustrated in Figure 3D. The absence of distinct  
10 and separated calcite nuclei could indicate that the calcite grew on ikaite or ACC surfaces  
11 without a separating double layer. “Complementary to these SAXS experiments, particle size and  
12 morphology were characterized ex-situ with SEM and TEM and these results indicate that in the  
13 50% CIT/Ca experiment, particle aggregates were more fine-grained (Figure 4A, B) and  
14 individual crystals were smaller (Figure 4C, D) compared to the 100% CIT/Ca.  
15  
16  
17  
18  
19  
20  
21  
22  
23  
24  
25  
26  
27  
28  
29  
30  
31



1  
2  
3 **Figure 4.** SEM (A) and TEM (B) of calcite formed after 2 hours with 50% CIT/Ca, and SEM (C)  
4 and TEM (D) of calcite formed after 1 hour with 100% CIT/Ca.  
5  
6  
7

8  
9 We summarized our findings in a schematic diagram (Figure 5). For both 50% and 100%  
10 CIT/Ca ratios, ACC aggregates with diameters larger than 100 nm formed almost  
11 instantaneously (Figure 5A). For the 50% CIT/Ca experiment, ACC transformed directly to  
12 calcite, without any other intermediate stages or any other metastable  $\text{CaCO}_3$  phases (Figure 5B,  
13 C). In contrast in the 100% CIT/Ca experiment, metastable ikaite formed and this transformed to  
14 calcite (Figure 5D-F).  
15  
16  
17  
18  
19  
20  
21  
22

23 The calcite that nucleated in the 50% CIT/Ca experiment formed as small nanoparticles as  
24 revealed by a small lobe in the SAXS-pattern, which was clearly distinguished from its  
25 underlying baseline (Figure 3A, B). Due to the simultaneous particle growth and formation of  
26 new particle nuclei, the polydispersity increased (Figure 3D, 5C), which explains the diminishing  
27 lobe in the SAXS curve (Figure 3B, from green arrow to red arrow).  
28  
29  
30  
31  
32  
33  
34  
35  
36  
37  
38  
39  
40  
41  
42  
43  
44  
45  
46  
47  
48  
49  
50  
51  
52  
53  
54  
55  
56  
57  
58  
59  
60

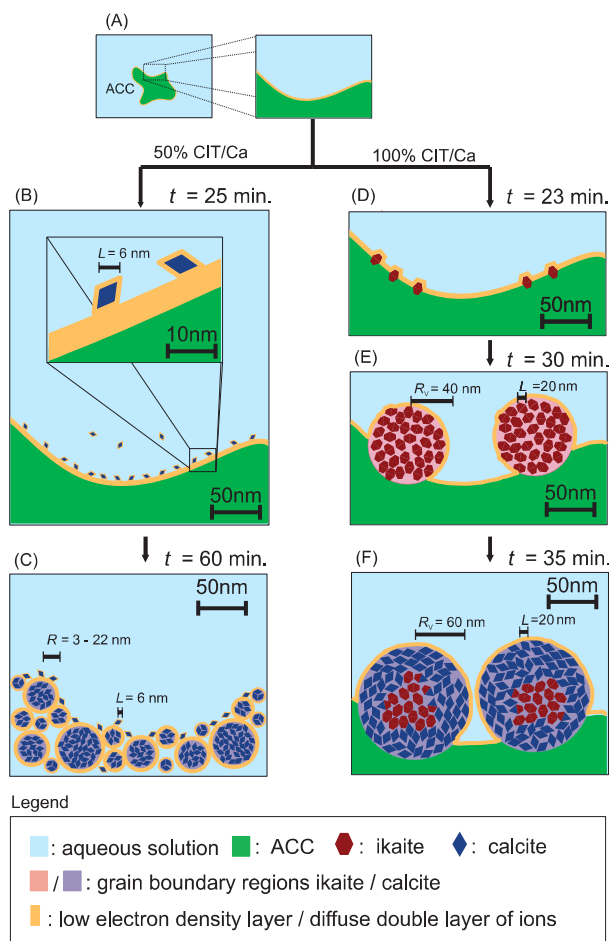


**Figure 5.** Illustration of particle formation for 50% and 100% CIT/Ca. (A) ACC particles were present immediately after mixing of the citrate/carbonate solution with the calcium solution for both CIT/Ca ratios. (B) In the 50% CIT/Ca experiment, nucleation of calcite nanoparticles was clearly visible in the SAXS pattern at 24 min. These calcite nanoparticles were potentially separated from the ACC particles by a low electron dense diffuse ion double layer, allowing them to be observed as individual entities within the SAXS pattern. (C) With time, a polydisperse mixture of calcite particles formed. No ikaite formed in this experiment. (D) In the 100% CIT/Ca, ikaite nanocrystallites formed at 23 min that could not be distinguished as individual nanoparticles within the SAXS pattern. (E) Fairly monodisperse particles of ikaite

1  
2  
3 crystals at 30 min just before calcite nucleated. (F) Mixed ikaite/calcite particles at 35 min after  
4  
5 mixing the solutions for 100% CIT/Ca.  
6  
7

8  
9 On the contrary, in the 100% CIT/ Ca experiment after ACC formation, only distinct  
10  
11 nanoparticles of ikaite formed and the degree of polydispersity was reduced as the ikaite particle  
12  
13 sizes grew with time (see lobes in the SAXS pattern Figure 3C). This change became more  
14  
15 pronounced as the reaction proceeded and the ikaite particles continued to grow, and eventually  
16  
17 when they started to transform after 30 min into calcite (Figure 5 D-F). Important to note is the  
18  
19 fact that calcite did not form separate particles, but the newly forming calcite crystals co-existed  
20  
21 with ikaite particle (Figure 5F). Thus, ikaite and calcite likely grew on top of each other without  
22  
23 diffuse double layers in between. This made it practically impossible to distinguish them as  
24  
25 individual particles in the SAXS or WAXS data. In the end stages of the reaction, all ikaite  
26  
27 particles transformed into fairly monodisperse calcite particles with an  $R_V = 95$  nm. Noteworthy  
28  
29 is that these sizes are roughly 8 times the sizes of the calcite particles that formed in the 50%  
30  
31 CIT/Ca experiment ( $R_V = 3-22$  nm).  
32  
33  
34  
35  
36

37  
38 In our experiment the ikaite-to-calcite formation is more complex than in previously reported  
39  
40 experiments, since ikaite was not the only source of  $\text{CaCO}_3$  for calcite formation. The highest  
41  
42 dissolution rate of ikaite was  $\approx 15$  times smaller than the calcite formation rate. Consequently,  
43  
44 the majority of  $\text{CaCO}_3$  for calcite formation originated from the dissolution of the initially  
45  
46 formed ACC and / or from remnant ions in solution. The so formed calcite and ikaite crystals are  
47  
48 highly porous and similar to glendonite-type calcite polymorphs. Due to their high surface areas  
49  
50 (see also Figure 4), such crystals are ideal seeds for further growth from  $\text{Ca}^{2+}$  and  $\text{CO}_3^{2-}$  in  
51  
52 solution. Thus, even though ikaite was formed as a minor phase in our experiments, it acted as a  
53  
54 seed crystal and likely played a crucial role in the calcite formation mechanism. The presence of  
55  
56  
57  
58  
59  
60

1  
2  
3 such seeding crystallites facilitated the formation of enlarged calcite crystallites ( $L = 20$  nm) at  
4  
5 100% CIT/Ca compared to the smaller calcite crystallite ( $L = 6$  nm) at 50% CIT/Ca, where no  
6  
7 ikaite formed. The increased calcite crystallite size for 100% CIT/Ca could potentially be  
8  
9 explained by the increased solubility of calcite at the higher CIT/Ca ratio. However, previous  
10  
11 experiments at 25 °C, where ACC transformed directly to calcite, without ikaite formation,  
12  
13 revealed that the calcite crystallite size decreases with an increase in CIT/Ca ratio, due to an  
14  
15 increasing calcite solubility.<sup>23</sup> This is the opposite trend to what is observed here at reduced  
16  
17 temperatures, further supporting that the presence of ikaite affected the final calcite crystallite  
18  
19 size by acting as seeding material.  
20  
21  
22  
23

24 As proposed by Sanchez-Pastor et al.<sup>18</sup> the pseudomorphic ikaite-to-calcite transition may  
25  
26 occur through an interface-coupled dissolution re-precipitation mechanism. However, our SAXS  
27  
28 experiments did not provide any indication of the existence of a low electron density liquid-like  
29  
30 interface that separates the calcite from the ikaite phase and facilitated its transformation  
31  
32 mechanism. If such a liquid interface existed, its electron density must be close to the electron  
33  
34 density of ikaite, as otherwise the SAXS-curves should provide evidence of its existence.  
35  
36 Possibly, such liquid interfaces may exist, but with a similar composition and consequently a  
37  
38 similar electron density as ikaite. This could mean that ikaite first melts to a highly  
39  
40 supersaturated solution of one mol  $[\text{Ca}^{2+} \cdot \text{CO}_3^{2-}]$  per 6 mol  $\text{H}_2\text{O}$  which subsequently immediately  
41  
42 recrystallised into calcite. There is probably no need for additional water to be present at the  
43  
44 ikaite-calcite interface, since the liquid interface can have the same composition as ikaite. This is  
45  
46 consistent with previous research showing that no additional water was required for the ikaite-to-  
47  
48 calcite transformation.<sup>18</sup> On the other hand the available amount of water in ACC is substantially  
49  
50 lower (typically  $\text{CaCO}_3 \cdot 1 \text{ H}_2\text{O}$ ). As a result the liquid interface between ACC and calcite  
51  
52  
53  
54  
55  
56  
57  
58  
59  
60

1  
2  
3 probably contains a higher water content than the adjacent ACC and calcite, which provided a  
4 more distinct contrast between the solids and the electron poor interface that separated them. As  
5  
6 a consequence we can observe the formation of separated calcite nanoparticles in the 50%  
7  
8 CIT/Ca experiment (in the absence of ikaite) with a distinct diffuse double layer, which had not  
9  
10 been observed for the 100% CIT/Ca experiment.  
11  
12  
13  
14  
15  
16  
17

## 18 **Conclusions**

19  
20 As shown before calcite crystallization was retarded in the presence of citrate as a  
21  
22 complexing/coordinating ligand in solution and consequently enhancing the lifetime of  
23  
24 amorphous calcium carbonate (ACC). In the 50% CIT/Ca experiment, nanosized calcite entities  
25  
26 ( $R_V = 2.4$  nm,  $L = 2.3$  nm) nucleated after 22 min, which were seeding a fine-grained spherulitic  
27  
28 calcite morphology with aggregated particles in a size range between  $3.5 < R < 22$  nm being  
29  
30 composed of crystallites with a size of typically  $L \approx 6$  nm.  
31  
32  
33

34 At 100% CIT/Ca, ikaite formed concomitant with ACC dissolution and prior to calcite  
35  
36 formation. Its formation was facilitated by the low temperature conditions and the presence of  
37  
38 chelating citrate ligands that analogous to phosphate ligands retard the formation of anhydrous  
39  
40  $\text{CaCO}_3$ . However, given the substantially lower transformation rate of ikaite versus the formation  
41  
42 rate of calcite, it seems that only a minority (max 6.4%) of calcite was formed via ikaite as an  
43  
44 intermediate. On the other hand, the pseudomorphic ikaite-to-calcite transition provide porous  
45  
46 calcite crystals (glendonite polymorph) being ideal (high-surface area) seeding crystal for further  
47  
48 crystallization from solution.  
49  
50  
51  
52

53 The mechanism of calcite formation with a 100% CIT/Ca ratio is strikingly different as  
54  
55 compared to the 50% CIT/Ca ratio. Unlike the 50% ratio, the 100% ratio did not reveal  
56  
57  
58  
59  
60

1  
2  
3 nucleation of nanosized calcite crystals ( $R_V = 2.4$  nm), instead yielding substantially larger  
4  
5 crystallite ( $L = 20$  nm) and particle size ( $R_V = 95$  nm). The enlarged calcite crystallite size of  
6  
7  
8 100% CIT/Ca is most likely be explained by the presence of glendonite (porous calcite form  
9  
10 ikaite as a parent) that serve as seeding crystallites  
11

## 12 13 14 **Acknowledgements**

15  
16 This work was funded by the Engineering and Physical Sciences Research Council (EPSRC)  
17  
18 program grant (EP/I001514/1) for the Materials Interface with Biology (MIB) Consortium. The  
19  
20 synchrotron work was funded via Diamond Light Source (grant number SM9904) to Juan Diego  
21  
22 Rodriguez-Blanco. J.D.R.B. and D.J.T. also acknowledge financial support by the NanoCARB  
23  
24 (PIEFGA-2013-624016) and MIRO (PIEF-GA-2013-624619) Marie Curie Intra-European  
25  
26 Fellowship (IEF), respectively. Moreover, this research was partially made possible by Marie  
27  
28 Curie grant from the European Commission in the framework of NanoSiAl Individual  
29  
30 Fellowship, Project No. 703015 to Tomasz Stawski. We are grateful to for the help provided by  
31  
32 Dr. James Douch on beamline I22.  
33  
34  
35  
36  
37  
38

## 39 **References**

- 40  
41 (1) Ridgwell, A.; Zeebe, R. E. *Earth Planet. Sci. Lett.* **2005**, *234*, 299–315.  
42  
43  
44 (2) Tegetoff, F. W. *Calcium Carbonate*, 1st ed.; Birkhäuser: Basel, 2002.  
45  
46  
47 (3) Rodriguez-Blanco, J. D.; Sand, K. K.; Benning, L. G. In *New Perspectives on Mineral*  
48  
49 *Nucleation and Growth: From Solution Precursors to Solid Materials*; Van Driessche, A. E. S.,  
50  
51 Kellermeier, M., Benning, L. G., Gebauer, D., Eds.; Springer International Publishing: Cham,  
52  
53 2017; pp 93–111.  
54  
55  
56  
57  
58  
59  
60

- 1  
2  
3 (4) Xiao, J.; Yang, S. *Nanoscale* **2012**, *4* (1), 54.  
4  
5  
6  
7 (5) Sand, K. K.; Rodriguez-Blanco, J. D.; Makovicky, E.; Benning, L. G.; Stipp, S. L. S.  
8  
9 *Cryst. Growth Des.* **2011**, *12*, 842–853.  
10  
11  
12 (6) Westin, K. J.; Rasmuson, A. C. *J. Colloid Interface Sci.* **2005**, *282* (2), 359–369.  
13  
14  
15 (7) Leeuw, N. H. De; Parker, S. C. *Faraday* **1997**, *93* (3), 467–475.  
16  
17  
18 (8) Harris, J.; Mey, I.; Hajir, M.; Mondeshki, M.; Wolf, S. E. *CrystEngComm* **2015**, *17*  
19  
20 (6831), 6767–7008.  
21  
22  
23  
24 (9) Beck, R.; Andreassen, J. *J. Cryst. Growth* **2010**, *312* (15), 2226–2238.  
25  
26  
27  
28 (10) Addadi, L.; Joester, D.; Nudelman, F.; Weiner, S. *Chem. Eur. J.* **2006**, *12*, 980–987.  
29  
30  
31 (11) Dauphin, Y.; Dufour, E. *Micron* **2008**, *39* (7), 891–896.  
32  
33  
34 (12) Tseng, Y.; Chevallard, C.; Dauphin, Y.; Guenoun, P. *Cryst. Eng. Comm.* **2014**, *16*, 561–  
35  
36 569.  
37  
38  
39 (13) Gower, L. A.; Tirrell, D. A. *J. Cryst. Growth* **1998**, *191*, 153–160.  
40  
41  
42  
43 (14) Seto, J.; Ma, Y.; Davis, S. A.; Meldrum, F.; Gourrier, A.; Kim, Y.-Y.; Schilde, U.;  
44  
45 Sztucki, M.; Burghammer, M.; Maltsev, S.; Jäger, C.; Cölfen, H. *Proc. Natl. Acad. Sci. U. S. A.*  
46  
47 **2012**, *109* (10), 3699–3704. (15) Shearman, D. J.; Smith, A. J. *Proc. Geol. Assoc.* **1985**, *96*  
48  
49 (4), 305–314.  
50  
51  
52  
53 (16) Swainson, I. P.; Hammond, R. P. *Mineral. Mag.* **2003**, *67* (3), 555–562.  
54  
55  
56  
57 (17) De Lurio, J. L.; Frakes, L. A. *Geochim. Cosmochim. Acta* **1999**, *63* (7–8), 1039–1048.  
58  
59  
60

- 1  
2  
3 (18) Sánchez-Pastor, N.; Oehlerich, M.; Astilleros, J. M.; Kaliwoda, M.; Mayr, C. C.;  
4  
5 Fernández-Díaz, L.; Schmahl, W. W. *Geochim. Cosmochim. Acta* **2016**, *175*, 271–281.  
6  
7  
8  
9 (19) Hellenbrandt, M. *Crystallogr. Rev.* **2004**, *10* (1), 37–41.  
10  
11  
12 (20) Downs, R. T.; Hall-Wallace, M. *Am. Mineral.* **2003**, *88*, 247–250.  
13  
14  
15 (21) Rickaby, R. E. M.; Shaw, S.; Bennitt, G.; Kennedy, H.; Zabel, M.; Lennie, A. *Geology*  
16  
17 **2006**, *34* (6), 497–500.  
18  
19  
20 (22) Rodriguez-Blanco, J. D.; Shaw, S.; Bots, P.; Benning, L. G. *J. Alloys Compd.* **2012**, *536*  
21  
22 (1), S477–S479.  
23  
24  
25 (23) Tobler, D. J.; Rodriguez-Blanco, J. D.; Dideriksen, K.; Bovet, N.; Sand, K. K.; Stipp, S.  
26  
27 *L. S. Adv. Funct. Mater.* **2015**, *25* (20), 3081–3090.  
28  
29  
30 (24) Mueller, M.; Wang, M.; Schulze-Briese, C. G. *Acta Crystallogr. Sect. D Biol.*  
31  
32 *Crystallogr.* **2012**, *68* (1), 42–56.  
33  
34  
35 (25) Huang, T. C.; Toraya, H.; Blanton, T. N.; Wu, Y.; IUCr. *J. Appl. Crystallogr.* **1993**, *26*  
36  
37 (2), 180–184.  
38  
39  
40 (26) Fratzl, P.; Misof, K.; Zizak, I.; Rapp, G.; Amenitsch, H.; Bernstorff, S. *J. Struct. Biol.*  
41  
42 **1998**, *122* (1), 119–122.  
43  
44  
45 (27) Zhang, F.; Ilavsky, J.; Long, G. G.; Quintana, J. P. G.; Allen, A. J.; Jemian, P. R. *Metall.*  
46  
47 *Mater. Trans. A* **2010**, *41* (5), 1151–1158.  
48  
49  
50 (28) Guinier, A. *X-ray Diffraction. In crystals Imperfect crystals, and Amorphous Bodies*;  
51  
52  
53  
54  
55  
56  
57  
58  
59  
60

1  
2  
3 (29) Bots, P.; Benning, L. G.; Rodriguez-Blanco, J.-D.; Roncal-Herrero, T.; Shaw, S. *Cryst.*  
4  
5 *Growth Des.* **2012**, *12* (7), 3806–3814.  
6  
7

8  
9 (30) Parkhurst, D.L., and Appelo, C.A.J., 2013. In *Description of input and examples for*  
10 *PHREEQC version 3—A computer program for speciation, batch-reaction, one-dimensional*  
11 *transport, and inverse geochemical calculations, available at: <https://pubs.usgs.gov/tm/06/a43/>;*  
12  
13 U.S. Geological Survey Techniques and Methods (2013).  
14  
15  
16  
17

18  
19 (31) Plummer, L. N.; Busenberg, E. *Geochim. Cosmochim. Acta* **1982**, *46* (6), 1011–1040.  
20  
21

22 (32) Brecevic, L.; Nielsen, A. E. *J. Cryst. Growth* **1989**, *98* (3), 504–510.  
23  
24

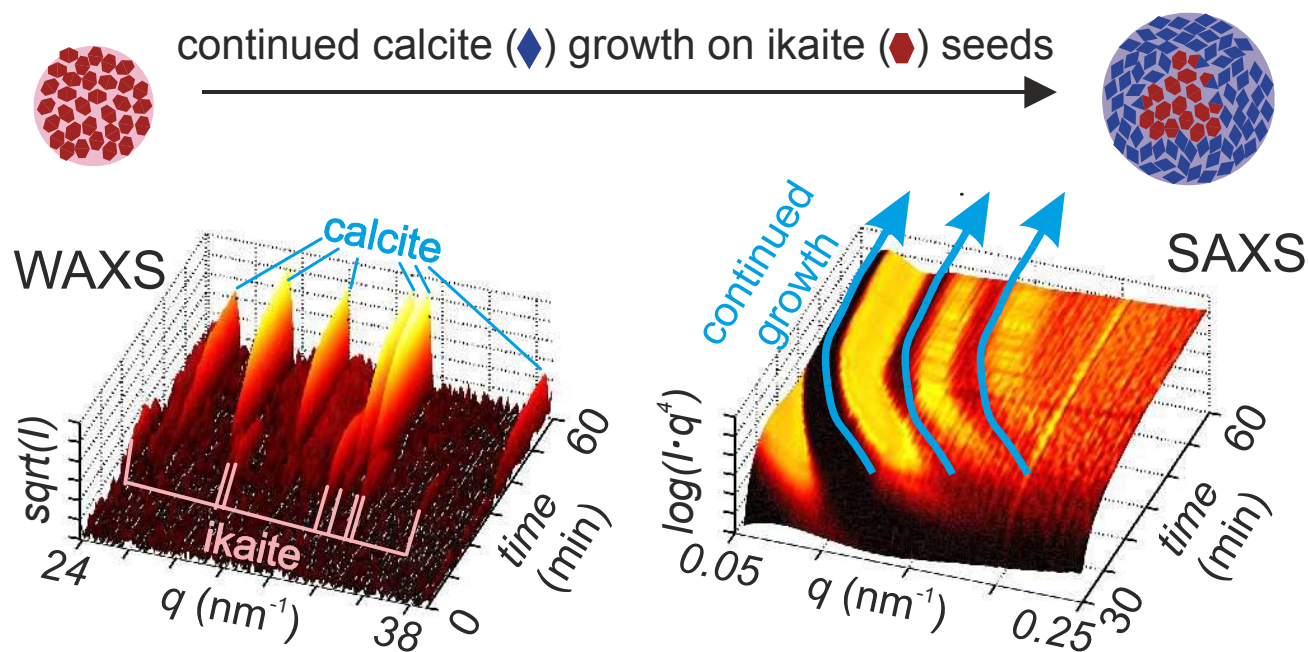
25 (35) Montanari, G; Rodriguez-Blanco; .J. D.; N. Bovet Stipp , S. L. S. and Tobler, D. J..  
26  
27 *Cryst. Growth Des.* (Article in press)  
28  
29  
30

31 (34) Kotlarchyk, M.; Chen, S.-H. *J. Chem. Phys.* **1983**, *79* (5), 2461.  
32  
33

34 (35) Raiteri, P.; Gale, J. D. *J. Am. Chem. Soc.* **2010**, *132* (6), 17623–17634.  
35  
36  
37  
38  
39  
40  
41  
42  
43  
44  
45  
46  
47  
48  
49  
50  
51  
52  
53  
54  
55  
56  
57  
58  
59  
60

**FOR TABLE OF CONTENTS USE ONLY:****How short-lived ikaite affects calcite crystallisation**

*R. Besselink, J.D. Rodriguez-Blanco, T. M. Stawski, L.G. Benning and D. J. Tobler*

**Synopsis:**

With a 100% citrate/Ca<sup>2+</sup> ratio the formation of calcite was preceded by short-lived ikaite at 5°C. This led to substantially larger calcite particle morphology and crystallite sizes in comparison to the 50% citrate/Ca<sup>2+</sup> ratio, where no ikaite was observed. Short-lived ikaite may have provided seeding crystals enhancing crystal growth of calcite.